Supernova Olivine from Cometary Dust

Scott Messenger,[1]* Lindsay P. Keller,[1] Dante S. Lauretta[2]

An interplanetary dust particle contains a submicrometer crystalline silicate aggregate of probable supernova origin. The grain has a pronounced enrichment in $^{18}O/^{16}O$ (13 times the solar value) and depletions in $^{17}O/^{16}O$ (one-third solar) and $^{29}Si/^{28}Si$ (<0.8 times solar), indicative of formation from a type II supernova. The aggregate contains olivine (forsterite 83) grains <100 nanometers in size, with microstructures that are consistent with minimal thermal alteration. This unusually iron-rich olivine grain could have formed by equilibrium condensation from cooling supernova ejecta if several different nucleosynthetic zones mixed in the proper proportions. The supernova grain is also partially encased in nitrogen-15–rich organic matter that likely formed in a presolar cold molecular cloud.

Primitive meteorites and interplanetary dust particles (IDPs) contain small amounts of micrometer-sized presolar grains (stardust) that originated from evolved stars, novae, and supernovae. These grains provide direct probes of astrophysical environments that are inaccessible to traditional astronomical techniques (*1*). Stardust identified to date includes grains of diamond, Si_3N_4, SiC, graphite, TiC, Al_2O_3, TiO_2, hibonite, spinel, forsterite, and amorphous silicates (*2*, *3*). Grains of extrasolar origin are identified by isotopic compositions that differ from solar isotopic ratios, in some cases by orders of magnitude.

Silicates are an abundant form of dust in the galaxy, giving rise to strong infrared (IR) spectral features in outflows of evolved stars (*4*, *5*), the diffuse interstellar medium (ISM) (*6*), and disks around young stellar objects (*7*). Silicates are identified by their diagnostic 9.7 μm and 18 μm IR bands due to Si-O stretch and O-Si-O bending modes. The general lack of fine structure in these bands is usually attributed to the silicate dust being primarily amorphous in the diffuse ISM, although some far-IR spectra have revealed the presence of ~10% to 20% crystalline silicates around young and old stars. The scarcity of crystalline silicates in the diffuse ISM (~0.2%) thus suggests that they are destroyed or rendered amorphous by shock, sputtering, or collision within ~10 million years after they form in stars (*6*, *8*). The discovery of presolar silicates in meteorites and IDPs provides new insight into interstellar silicate mineralogy. To date, 6 of the 132 presolar silicates found thus far have been studied by transmission electron microscopy (TEM), including 2 forsterite grains and 4 amorphous silicates (*3*, *9–11*, this work).

Although silicates are the most abundant type of presolar grains, they were only discovered recently because of their small size (0.1 to 1.0 μm) and the difficulty in locating them among the overwhelming background of solar system silicates in meteorites. Silicate stardust is more abundant in anhydrous IDPs [450 to 5500 parts per million (ppm)] than in meteorites [<300 parts per billion (ppb) to 180 ppm] (*3*, *10*, *12–17*) and micrometeorites (300 ppm) (*9*). Many anhydrous IDPs also harbor discrete μm-sized concentrations of molecular cloud matter, marked by highly elevated D/H and $^{15}N/^{14}N$ ratios (*18*, *19*). The greater survival of presolar materials in anhydrous IDPs shows that these are the least altered remnants of the early solar system, lending support to the view that these IDPs are samples of short-period comets (*20*, *21*).

Here, we report the identification of a silicate grain with a probable origin from a type II supernova. The 500-nm grain (B10A) was identified in five (30 to 70 nm thick) serial sections of an anhydrous cluster IDP (L2011B10) by oxygen isotopic imaging with the Washington University NanoSIMS 50 ion microprobe (*22*). The grain was first identified in O isotopic images of an Au-mounted section, where it was found to have a $^{18}O/^{16}O$ ratio of 13 times the solar value and a $^{17}O/^{16}O$ ratio of one-third that of the solar ratio ($^{18}O/^{16}O = 2.7 \pm 0.1 \times 10^{-2}$, $^{17}O/^{16}O = 1.1 \pm 0.2 \times 10^{-4}$; 1 SD). Simultaneously acquired $^{28}Si^-$ and $^{24}Mg^{16}O^-$ images showed the grain to be a Mg-rich silicate. In an adjacent slice of the IDP, B10A was found to have an anomalous Si isotopic composition [$\delta^{29}Si = -224 \pm 54$ per mil (‰), $\delta^{30}Si = -23 \pm 104$ ‰; 1 SD] (*23*). Because the grain was much smaller in this section (<200 nm), its measured $^{18}O/^{16}O$ ratio ($7.5 \pm 2 \times 10^{-3}$) was significantly influenced by nearby isotopically solar material (*24*). The observed Si isotopic anomaly should thus be considered a lower limit to the grain's true composition. Fe and Mg isotopic measurements were not possible because too little material was available.

Most presolar oxides and silicates fall within four isotopic groups (*25*), pointing to origins in low- to intermediate-mass red giant (RG) and asymptotic giant branch (AGB) stars of differing mass, age, and chemical composition (Fig. 1). In those stars, the onset of abundant dust formation occurs after deep convection brings nucleosynthetically processed material to the stellar surface. The strong ^{17}O enrichments and ^{18}O depletions of group 1 and group 2 grains are due to H burning in the CNO cycle, and the stronger ^{18}O depletions of group 2 grains are ascribed to extra mixing of material at the base of the convective envelope (*26*, *27*). The moderately ^{16}O-rich compositions of group 3 grains are thought to reflect origins from low metallicity RG and AGB stars. The group 4 grains are more enigmatic, but their moderately ^{17}O- and ^{18}O-rich compositions could reflect origins from high metallicity AGB stars. Two exceptional corundum grains have been proposed to originate from type II supernovae (*28*, *29*).

The O isotopic composition of grain B10A falls well outside the range of all previously studied presolar oxides and silicates. The pronounced ^{18}O enrichment is a signature of He burning, where abundant ^{18}O is produced through $^{14}N(\alpha,\gamma)^{18}F(e^+\nu)^{18}O$. The competing reaction $^{18}O(\alpha,\gamma)^{22}Ne$ destroys ^{18}O with increasing efficiency as burning progresses to higher temperatures, resulting in strong variations in the $^{18}O/^{16}O$ ratio of stars of differing mass and age. Abundant ^{12}C is also produced (by 3-α reactions) during He burning, resulting in high C/O ratios at the site where ^{18}O is produced. Although it is possible that ^{18}O-rich material is dredged up during the early evolution of some AGB stars, it must be mixed with the overlying O-rich H envelope to form silicates, leading to a ^{17}O-rich composition instead of the observed ^{17}O depletion. Massive Wolf-Rayet stars may also directly expose ^{18}O-rich products of partial He burning at the stellar surface during the WN-WC transition. However, we do not favor such an origin for this grain because of the high C/O ratio of the ^{18}O-rich ejecta.

The Si isotopic composition of B10A falls near the distribution of X-type SiC grains that have been shown to originate from supernovae (Fig. 2) and is clearly distinct from the far more abundant mainstream SiC grains that derive from RG and AGB stars. Furthermore, the ^{29}Si

[1]Mail Code KR, Robert M. Walker Laboratory for Space Science, NASA Johnson Space Center, Houston, TX 77058, USA. [2]Lunar and Planetary Laboratory, University of Arizona, Tucson, AZ 85721, USA.

*To whom correspondence should be addressed. E-mail: scott.r.messenger@nasa.gov

deficit of B10A is not consistent with an origin from a Wolf-Rayet star, as the ejecta is ^{30}Si and, to a lesser extent, ^{29}Si enriched (30).

The O and Si isotopic compositions of B10A point to an origin from a type II supernova. Type II supernovae occur when the core of a massive (>8 $M_\odot$) star collapses and explodes. The structure of a presupernova star consists of concentric compositionally distinct layers undergoing different nucleosynthetic burning stages (31), overlain by a massive H-rich convective envelope that experienced partial H burning at its base (32). The supernova drives explosive nucleosynthesis in the innermost zones that are subsequently marked by exotic and heterogeneous isotopic compositions. Supernovae produce copious amounts of ^{16}O and thus have low $^{17}O/^{16}O$ ratios relative to solar ratios (33). The relative yield of ^{18}O varies with stellar mass; it is moderately elevated among lower mass supernovae (for M < 15$M_\odot$) and low among higher mass supernovae (33).

The isotopic composition of B10A can only be reproduced by a mixture of material from different nucleosynthetic zones. Although B10A has a high $^{18}O/^{16}O$ ratio (13 times solar), the $^{18}O/^{16}O$ ratio of the He/C shell is typically 500 to 1000 times solar. Most of the O must have originated from the deeper shells with high relative amounts of ^{16}O (O/C, O/Ne, O/Si, or Si/S), because the low $^{17}O/^{16}O$ ratio excludes a major contribution from the H/He envelope. Further, the He/C shell is ^{28}Si poor, whereas B10A is ^{28}Si rich. Most of the Si atoms must have originated from the deepest (Si/S, Ni) zones.

TEM investigation found that the material surrounding the supernova grain contains sub-micrometer forsterite, enstatite, and GEMS grains (glass with embedded metal and sulfides) embedded in carbonaceous material. To unambiguously distinguish which (if any) of the grains were related to the supernova silicate, we imaged this area for $^{16}O^-$, $^{18}O^-$, and $^{32}S^-$, where sulfur was used to mark the location of the GEMS and FeS grains to help align the isotopic and TEM images. As shown in Fig. 3, A to C, the supernova grain is identified as a polycrystalline aggregate of forsterite. The nearby GEMS grains do not share the anomalous isotopic signature, leaving their origins uncertain.

In the thin section studied by TEM in detail, the supernova grain consisted of three discrete elongate lobes <250 nm in size. The lobes are polycrystalline, with well-defined subgrains (50 to 100 nm) that exhibit equilibrium grain boundaries in dark-field images (Fig. 4). Notably, this sub-μm polycrystalline morphology was also recently found in supernova SiC grains (34). The subgrains are identified as olivine on the basis of energy-dispersive x-ray analyses showing olivine stoichiometry [Mg/(Mg+Fe) atom ratio of 0.83 ± 0.01] and diffraction spacings characteristic of forsterite. Individual diffraction spots are well defined, with no evidence for streaking or asterism that would indicate extensive disorder (e.g., defects) in the crystalline lattice. We did not observe nuclear particle tracks or substantial (>10 nm) amorphous rims on the grains. There is no apparent crystallographic relationship among the subgrains.

Overall, the microstructure of the grain suggests that the individual crystallites formed separately by condensation before aggregating. The equilibrium grain boundaries between the crystallites are consistent with limited thermal annealing of the grains; however, the thermal event was not long enough or hot enough to completely recrystallize the subgrains. The annealing event may also have erased an earlier radiation history, but the extent of any prior radiation processing was not extensive enough to alter the grain's chemistry substantially.

The identification of B10A as an aggregate of Fe-bearing olivine provides additional constraints on its origin. Many different mixtures of nucleosynthetic zones satisfy the observed isotopic constraints, but most mixtures result in chemical compositions incompatible with olivine condensation. Supernovae are also dynamic, radiation-rich environments that may defy standard views of equilibrium grain condensation. Clayton et al. (35, 36) have argued that in supernovae the critical CO molecule is efficiently disrupted by Compton electrons produced by the decay of short-lived nuclides (especially ^{56}Co), resulting in abundant, free neutral C and O atoms. Their model suggests that graphite may condense from such a gas even when C/O < 1 and that oxides may condense from a gas where C/O > 1. Although

Fig. 1. O isotopic composition of grain B10A compared with previously reported values of presolar corundum (25, 28, 29, 59–61) and silicates (3, 12–15). Two corundum grains identified in the figure as Choi98 and Nittler98 are thought to originate from type II supernovae (28, 29).
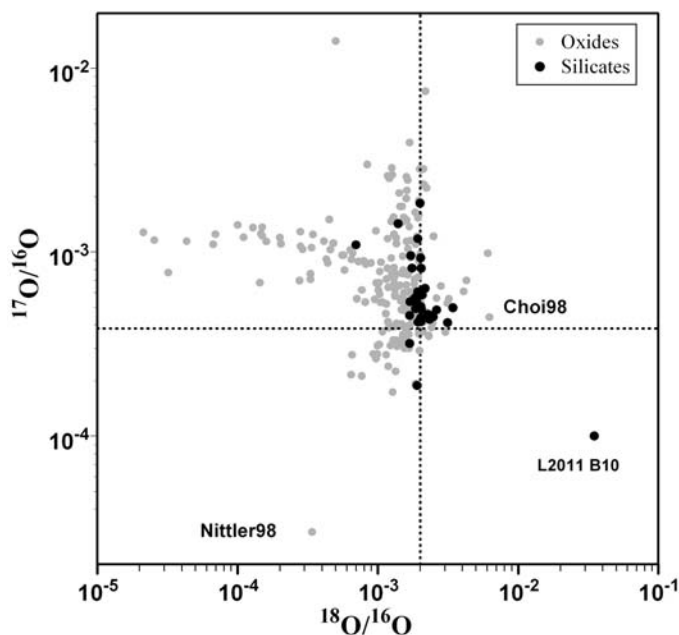

Fig. 2. Si isotopic composition of grain B10A compared with previously analyzed SiC and graphite grains (62–67). The Si measurement was compromised by surrounding isotopically solar material, and the true composition is likely to be more anomalous. The Si isotopic composition is most similar to X-type SiC grains that are thought to derive from supernovae. The mainstream SiC grains and other minor isotopic subgroups (A, B, Y, and Z grains) account for ~98% of all SiC and are thought to originate from low-mass RG and AGB stars.
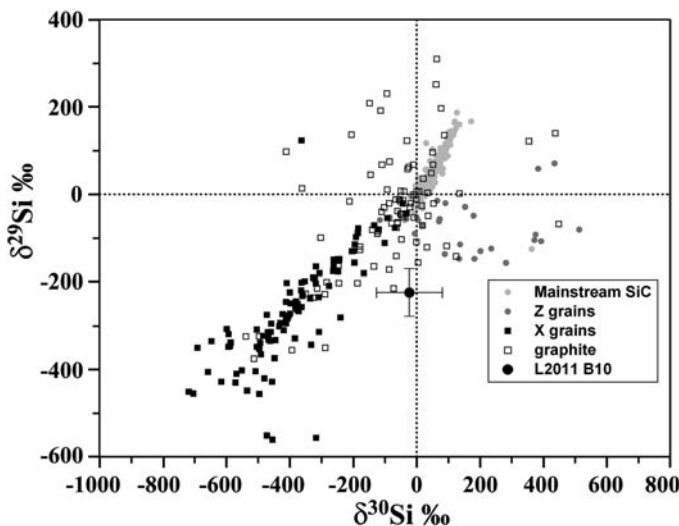
B10A is unlikely to have formed from a C-rich gas (based on its $^{18}O/^{16}O$ ratio), the availability of more abundant, free O would have resulted in an enhanced O fugacity that would have helped produce abundant oxidized iron. This unusual circumstance results in an environment more conducive to Fe uptake in condensing olivine (37).

Different mixtures of postexplosion zonal compositions were generated from 15 to 25 $M_\odot$ solar metallicity supernovae in appropriate proportions to match the O and Si isotopic composition of B10A (22). We explored the equilibrium condensation chemistry of chemical systems with these compositions. In addition, we evaluated the effect of inhibited CO-molecule formation on the condensation chemistry of the system. Our approach is similar to that in (38). The system was held at a constant pressure of 10^{-5} bars, and temperature varied from 500 to 2000 K. Thermodynamic data sources and computational techniques are described in (39) and (22).

From the available nucleosynthetic models, the best match to the isotopic constraints is a mixture comprised of 81 ± 4% He/C zone, 18 ± 1% O/C zone, 0.3 ± 0.02% Si/S zone, and 0.3 ± 0.02% Ni zone of a solar metallicity 15 $M_\odot$ supernova, where the uncertainties reflect ranges in composition consistent with the available constraints. Some elemental abundances of this mixture are distinctly different from those in a solar-composition system. In particular, the H/He ratio is $\sim 10^{-7.2}$, the C/O ratio is 0.89, and C and O are enriched, relative to Si, by factors of 12 and 7, respectively. The abundances of N, Mg, S, Ca, and Fe, relative to Si, are similar to those in a solar-composition system, whereas Al is depleted by $\sim 50\%$.

Diopside is the first major condensate in this system (22). However, olivine is by far the most abundant silicate, condensing at 1560 K as nearly pure forsterite ($Fo_{99.6}$). Lesser amounts of enstatite also form, reaching one-half the olivine abundance. The mole fraction of fayalite in olivine increases at lower temperatures, reaching a maximum value of 0.17 at 1250 K, where the incorporation of Fe into olivine is halted as a result of FeS condensation. The olivine composition remains relatively constant over a large temperature range, decreasing to a value of Fo_{91} at 950 K.

Remarkably, this chemical mixture is an exact match to both the isotopic composition of the grain and the Fe content of the olivine. We were unable to find similarly good matches from any zonal mixtures of higher mass supernovae owing to their lower production of ^{18}O relative to ^{16}O in the He/C shell, but lower mass supernovae may be alternate sources. Our model enables us to make the following inferences for the Mg and Fe isotopic composition of the olivine grain that were unfortunately not possible to measure owing to the small amount of material available:

$^{25}Mg/^{24}Mg \sim 12 \times$ solar, $^{26}Mg/^{24}Mg \sim 9 \times$ solar, $^{54}Fe/^{56}Fe \sim$ solar, $^{57}Fe/^{56}Fe \sim 2 \times$ solar, $^{58}Fe/^{56}Fe \sim 8 \times$ solar. The prominently elevated $^{25}Mg/^{24}Mg$ and $^{26}Mg/^{24}Mg$ ratios result from He burning in the O/C shell. The strong enrichment in $^{58}Fe/^{56}Fe$ is a result of slow neutron-capture reactions (s process) in the O/C and He/C shells.

This mixing model and resultant gas composition are not a unique solution, but isotopic constraints require that most of the gas must have been derived from the He/C shell, most ($\sim 97\%$) of the O atoms were derived from interior zones relatively rich in ^{16}O, and a large fraction of the Si atoms originated in the deepest ^{28}Si-rich zones. A substantial contribution of envelope material is also excluded because of its enrichment in $^{17}O/^{16}O$. Furthermore, material from the Si/S and Ni zones must have been mixed into the He/C zone without introducing much of the intervening layers. These

conclusions are in line with earlier studies of supernova graphite (40), SiC (41), and oxide (29) grains, whose isotopic compositions could only be reproduced by partial mixing of multiple nucleosynthetic zones.

We also investigated the effect of the radiation-rich environment on the condensation chemistry by inhibiting the formation of CO and of all gas-phase molecules. In this case, SiO was the first phase to condense. The increased O fugacity resulted in olivine condensing at higher temperature and a higher uptake of Fe. However, the gas is so oxidizing that this phase is very unstable, and most of the Fe in the olivine is lost as a result of the condensation of wüstite.

Observations of supernova 1987A showed that there was extensive large-scale mixing of material (42), in support of the story told by supernova stardust grains. It is unclear, though, how the large-scale overturn of material results

Fig. 3. (A) Transmission electron micrograph of a 4 by 4 μm region IDP L2011 B10 found to contain the presolar olivine grain. (B) The ^{18}O-rich region of the NanoSIMS isotopic image is overlain, showing that the supernova olivine is made of three distinct lobes. Other portions of the O isotopic image exhibit solar isotopic composition. (C) The blue regions show the S hotspots observed by NanoSIMS during the O isotopic image acquisition. These S-rich regions correspond to GEMS grains and small FeS grains. The S-rich spot in the lower left is due to a nearby sulfide; it is not aligned because the thin section stretched upon transfer to the NanoSIMS mount. (D) The color overlay shows the location of ^{15}N-rich material as observed in $^{12}C^{14}N$ and $^{12}C^{15}N$ isotopic images.
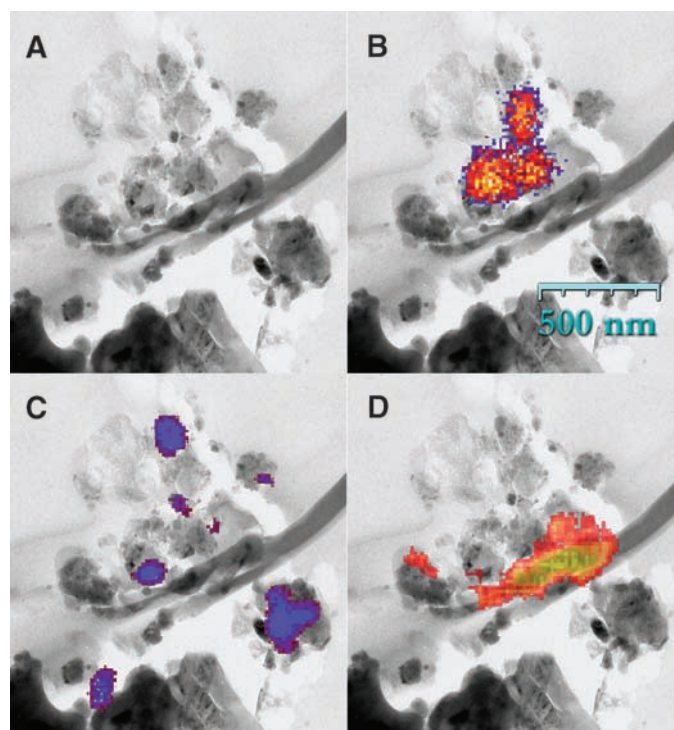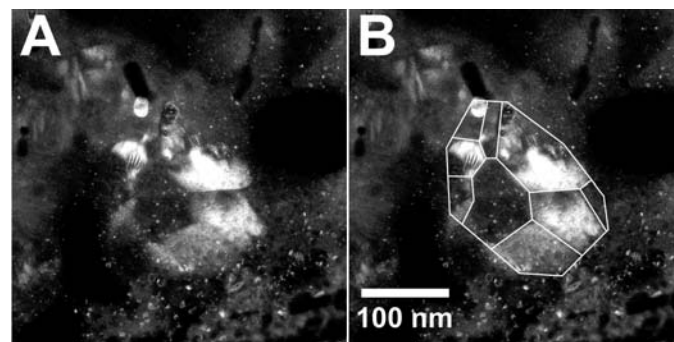

Fig. 4. (A) Dark-field TEM image of supernova olivine grain B10A. (B) White lines illustrate observed equilibrium grain boundaries between crystallites. Nanometer-sized white specks are due to residual Au coating used to minimize sample charging.

in microscopic mixing of multiple nucleo-synthetic zones on a time scale consistent with grain condensation (1 to 2 years).

Deneault et al. (43) recently suggested that some of this difficulty could be alleviated by implanting material after the grains had formed in reverse shock, possibly accounting for the abundant trace Fe in SiC X grains (44). However, this process could not generate the high, uniform abundance of Fe in B10A, because any implanted Fe atoms would have had to remove an equivalent number of Mg atoms to preserve the observed olivine stoichiometry.

Interstellar dust grains accrete coatings of mixed H_2O/organic ices in cold molecular clouds (45), and these ices may undergo extensive chemical processing driven by ultraviolet photolysis (e.g., 46) to become protective coatings of refractory organic matter (47). Interestingly, grain B10A is partially embedded in carbonaceous matter. As shown in Fig. 3D, this material has a high $^{15}N/^{14}N$ ratio ($\delta^{15}N$ = +471 ± 30 ‰), like values observed in organic matter in primitive meteorites and IDPs (48–50). The origin of the ^{15}N enrichment is thought to reflect isotopic fractionation during extremely low-temperature (<20 K) chemical reactions in a presolar cold molecular cloud environment (e.g., 51). This association of ^{15}N-rich organic matter with stardust has recently been reported for other presolar silicates (15), supporting a presolar origin for the N isotopic anomaly.

The well-preserved microstructure of B10A is not easily reconciled with the current understanding of grain processing in the ISM, which is expected to rapidly destroy or render crystalline silicates amorphous. It is possible that the 250-nm-thick layer of presolar organic matter shielded the grain from extensive radiation damage and may also have protected the grain from supernova shocks that act as the primary destruction mechanism for interstellar grains. However, the isotopic signature of the coating is characteristic of a cold molecular cloud environment and thus may not have been present during the grain's initial transit through the diffuse ISM.

Alternatively, this grain may have had an unusually short residence time in the ISM. Interstellar grain lifetimes are estimated to be 200 to 400 million years (52, 53). On the basis of the disparity between the observed abundances of crystalline silicates in evolved stars and the diffuse ISM, crystalline silicates may survive less than 10 million years in this environment (8). If this is the case, the parent supernova of B10A may have occurred relatively close to the site of our Sun's formation. The recent demonstration that abundant ^{60}Fe ($t_{1/2}$ = 1.5 million years) was live in the early solar system establishes that there was a late addition of recently synthesized stellar ejecta into the solar nebula—either a type II supernova or an AGB star (54, 55). This must have

occurred within a few lifetimes after the ^{60}Fe was produced, consistent with the estimated lifetime of B10A in the diffuse ISM. Although either source is possible, the timing of an AGB star passing near the Sun would have been fortuitous, whereas the solar system is likely to have formed in a massive stellar nursery that was populated by massive O, B stars that quickly evolve and perish as supernovae (56).

Because this is the first presolar silicate grain of probable supernova origin among the 132 presolar silicates reported thus far, the relative contribution of supernova silicates appears to be ~1%. This is roughly consistent with the far better known abundance of supernova SiC grains (1%) and Al_2O_3 grains (1%), but much lower than the fraction of presolar graphite thought to originate from supernovae (>30%). These numbers do not support the recent suggestion that type II supernovae are a dominant source of dust in the galaxy, based on observations of the Cassiopeia A supernova remnant (57).

References and Notes

1. T. J. Bernatowicz and E. Zinner, Eds., *Astrophysical Implications of the Laboratory Study of Presolar Materials* (AIP Conf. Proc. 402, American Institute of Physics, Woodbury, NY, 1998).
2. E. Zinner, in *Treatise on Geochemistry*, K. K. Turekian, H. D. Holland, v. e. A. M. Davis, Eds. (Elsevier, Oxford, 2004), vol. 1, pp. 17–39.
3. S. Messenger, L. P. Keller, F. J. Stadermann, R. M. Walker, E. Zinner, *Science* **300**, 105 (2003).
4. L. B. F. M. Waters et al., *Astron. Astrophys.* **315**, L361 (1996).
5. F. Kemper, F. J. Molster, C. Jäger, L. B. F. M. Waters, *Astron. Astrophys.* **394**, 679 (2002).
6. F. Kemper, W. J. Vriend, A. G. G. M. Tielens, *Astrophys. J.* **609**, 826 (2004).
7. G. Meeus et al., *Astron. Astrophys.* **365**, 476 (2001).
8. E. F. van Dishoeck, *Annu. Rev. Astron. Astrophys.* **42**, 119 (2004).
9. T. Yada et al., *Lunar Planet. Sci.* **36**, abstr. 1227 (2005).
10. A. Nguyen, E. Zinner, R. Stroud, A. Nguyen, *Lunar Planet. Sci.* **36**, abstr. 2196 (2005).
11. Three of the four amorphous presolar silicate grains found thus far are categorized as GEMS grains (glass with embedded metal and sulfides), materials that comprise a major component of cometary/anhydrous IDPs, occasionally exceeding 50 weight % of the IDP. GEMS grains are typically 0.1 to 0.5 µm in size, have approximately chondritic elemental abundances (with the exception of C), and have optical properties consistent with those observed for interstellar amorphous silicates (58).
12. A. Nguyen, E. Zinner, *Science* **303**, 1496 (2004).
13. K. Nagashima, A. N. Krot, H. Yurimoto, *Nature* **428**, 921 (2004).
14. S. Mostefaoui, P. Hoppe, *Astrophys. J.* **613**, L149 (2004).
15. C. Floss, F. J. Stadermann, *Lunar Planet. Sci.* **35**, abstr. 1281 (2004).
16. S. Kobayashi et al., *Lunar Planet Sci.* **36**, abstr. 1931 (2005).
17. P. Hoppe, S. Mostefaoui, T. Stephan, *Lunar Planet. Sci.* **36**, abstr. 1301 (2005).
18. S. Messenger, R. M. Walker, in *Astrophysical Implications of the Laboratory Study of Presolar Materials*, T. J. Bernatowicz, E. Zinner, Eds. (AIP Conf. Proc. 402, American Institute of Physics, Woodbury, NY, 1998), pp. 545–564.
19. S. Messenger, *Nature* **404**, 968 (2000).
20. J. P. Bradley, S. A. Sandford, R. M. Walker, in *Meteorites and the Early Solar System*, J. Kerridge, M. S. Matthews, Eds. (Univ. of Arizona Press, Tucson, AZ, 1988), pp. 861–895.

21. S. Messenger, *Meteor. Planet. Sci* **37**, 1491 (2002).
22. Materials and methods are available as supporting material on *Science* Online.
23. Delta values represent the deviation of the measured isotopic ratio from the terrestrial standard, in parts per thousand (‰); $\delta R = \left(\frac{R \text{ measured}}{R \text{ standard}} - 1 \right) \times 1000$.
24. In this case, we acquired $^{16,18}O-$ and $^{28,29,30}Si-$ isotopic images with an estimated spatial resolution of 100 nm. The grain only appeared in the first 3 of the 10 image scans, with an apparent maximum size of 250 nm. By comparing the $^{18}O/^{16}O$ ratio measured in this section (0.0075 ± 0.002, 2 SD) with that of the largest (500 nm) piece ($^{18}O/^{16}O$ = 0.027 ± 0.002, 2 SD), we estimate that nearby material contributed between 69 and 85% of the O ions counted (where the range arises from the uncertainty in the measured $^{18}O/^{16}O$ ratio). If a similar degree of contamination affected the Si data ($\delta^{29}Si$ = −224 ± 108 ‰, $\delta^{30}Si$ = −23 ± 208 ‰; 2 SD), we infer that the true $\delta^{29}Si$ lies between −370 and −1000 ‰. The uncertainty in the $\delta^{30}Si$ value (100 ‰) is too great to permit a similar inference of its true isotopic composition.
25. L. R. Nittler, C. M. O'D. Alexander, X. Gao, R. M. Walker, E. Zinner, *Astrophys. J.* **483**, 475 (1997).
26. A. I. Boothroyd, I.-J. Sackmann, *Astrophys. J.* **510**, 232 (1999).
27. D. D. Clayton, L. R. Nittler, in *Origin and Evolution of the Elements*, A. McWilliam, T. Rauch, Eds. (Carnegie Observatory Astrophysics Series, Pasadena, CA, 2004), pp. 297–316.
28. L. R. Nittler, C. M. O'D. Alexander, J. Wang, X. Gao, *Nature* **393**, 222 (1998).
29. B.-G. Choi, G. R. Huss, G. J. Wasserburg, R. Gallino, *Science* **282**, 1284 (1998).
30. M. Arnould, G. Meynet, G. Paulus, in *Astrophysical Implications of the Laboratory Study of Presolar Materials*, T. J. Bernatowicz, E. Zinner, Eds. (AIP Conf. Proc. 402, American Institute of Physics, Woodbury, NY, 1998), pp. 179–202.
31. B. S. Meyer, T. A. Weaver, S. E. Woosley, *Meteoritics* **30**, 325 (1995).
32. S. E. Woosley, T. A. Weaver, *Astrophys. J. Suppl.* **101**, 181 (1995).
33. T. Rauscher, A. Heger, R. D. Hoffman, S. E. Woosley, *Astrophys. J.* **576**, 323 (2002).
34. R. M. Stroud, L. R. Nittler, P. Hoppe, *Met. Planet. Sci.* **39**, abstr. 5039 (2004).
35. D. D. Clayton, W. Liu, A. Dalgarno, *Science* **283**, 1290 (1999).
36. D. D. Clayton, E. A.-N. Deneault, B. S. Meyer, *Astrophys. J.* **562**, 480 (2001).
37. A. V. Fedkin, L. Grossman, *Lunar Planet. Sci.* **35**, A1823 (2004).
38. D. S. Ebel, L. Grossman, *Geochim. Cosmochim. Acta* **64**, 339 (2000).
39. M. A. Pasek et al., *Icarus* **175**, 1 (2005).
40. C. Travaglio et al., *Astrophys. J.* **510**, 325 (1999).
41. S. Amari, P. Hoppe, E. Zinner, R. S. Lewis, *Astrophys. J.* **394**, L43 (1992).
42. D. H. Wooden, in *Astrophysical Implications of the Laboratory Study of Presolar Materials*, T. J. Bernatowicz, E. Zinner, Eds. (AIP Conf. Proc. 402, American Institute of Physics, Woodbury, NY, 1998), pp. 317–376.
43. E. A.-N. Deneault, D. D. Clayton, A. Heger, *Astrophys. J.* **594**, 312 (2003).
44. K. K. Marhas, P. Hoppe, A. Besmehn, *Lunar Planet. Sci.* **35**, abstr. 1834 (2004).
45. E. L. Gibb et al., *Astrophys. J.* **536**, 347 (2000).
46. M. P. Bernstein, *Astrophys. J.* **576**, 1115 (2002).
47. A. Li, J. M. Greenberg, *Astron. Astrophys.* **323**, 566 (1997).
48. C. M. O'D Alexander et al., *Met. Planet. Sci.* **33**, 603 (1998).
49. L. P. Keller et al., *Geochim. Cosmochim. Acta* **68**, 2577 (2004).
50. C. Floss et al., *Science* **303**, 1355 (2004).
51. S. B. Charnley, S. D. Rodgers, *Astrophys. J.* **569**, L133 (2002).
52. A. P. Jones, A. G. G. M. Tielens, D. J. Hollenbach, *Astrophys. J.* **469**, 740 (1996).
53. H. Mouri, Y. Taniguchi, *Astrophys. J.* **534**, L63 (2000).
54. S. Tachibana, G. R. Huss, *Astrophys. J.* **588**, L41 (2003).
55. M. Busso, R. Gallino, G. J. Wasserburg, *Publ. Astron. Soc. Aust.* **20**, 356 (2003).

56. C. J. Lada, E. A. Lada, *Annu. Rev. Astron. Astrophys.* **41**, 57 (2003).
57. L. Dunne, S. Eales, R. Ivison, H. Morgan, M. Edmunds, *Nature* **424**, 285 (2003).
58. J. P. Bradley *et al.*, *Science* **285**, 1716 (1999).
59. B.-G. Choi, G. J. Wasserburg, G. R. Huss, *Astrophys. J.* **522**, L133 (1999).
60. H. Krestina, W. Hsu, G. J. Wasserburg, *Lunar Planet. Sci.* **33**, abstr. 1425 (2002).
61. E. Zinner *et al.*, *Geochim. Cosmochim. Acta* **67**, 5083 (2004).
62. C. M. O'D. Alexander, *Geochim. Cosmochim. Acta* **57**, 2869 (1993).
63. P. Hoppe, S. Amari, E. Zinner, T. Ireland, R. S. Lewis, *Astrophys. J.* **430**, 870 (1994).
64. P. Hoppe, S. Amari, E. Zinner, R. S. Lewis, *Geochim. Cosmochim. Acta* **60**, 883 (1996).
65. G. R. Huss, I. D. Hutcheon, G. J. Wasserburg, *Geochim. Cosmochim. Acta* **61**, 5117 (1997).
66. S. Amari *et al.*, *Astrophys. J.* **546**, 248 (2001).
67. S. Amari, L. R. Nittler, E. Zinner, K. Lodders, R. S. Lewis, *Astrophys. J.* **559**, 463 (2001).
68. This is the inaugural paper from the newly established Robert M. Walker Laboratory for Space Science at Astromaterials Research and Exploration Science, NASA Johnson Space Center. This research was supported by NASA Cosmochemistry grants to S.M., L.P.K., and D.S.L. This work was enabled by the NanoSIMS ion microprobe designed by G. Slodzian. We thank A. Heger and S. Woosley for generously sharing unpublished supernova model data. The revision of this paper benefited from careful reviews by two anonymous reviewers.

Cytokinin Oxidase Regulates Rice Grain Production

Motoyuki Ashikari,[1]* Hitoshi Sakakibara,[2]* Shaoyang Lin,[3] Toshio Yamamoto,[3] Tomonori Takashi,[3] Asuka Nishimura,[3] Enrique R. Angeles,[3] Qian Qian,[4] Hidemi Kitano,[1] Makoto Matsuoka[1]†

Most agriculturally important traits are regulated by genes known as quantitative trait loci (QTLs) derived from natural allelic variations. We here show that a QTL that increases grain productivity in rice, *Gn1a*, is a gene for cytokinin oxidase/dehydrogenase (OsCKX2), an enzyme that degrades the phytohormone cytokinin. Reduced expression of *OsCKX2* causes cytokinin accumulation in inflorescence meristems and increases the number of reproductive organs, resulting in enhanced grain yield. QTL pyramiding to combine loci for grain number and plant height in the same genetic background generated lines exhibiting both beneficial traits. These results provide a strategy for tailormade crop improvement.

Food shortage is one of the most serious global problems in this century. The United Nations Food and Agricultural Organization (FAO) estimates that 852 million people worldwide were undernourished in 2000 to 2002 (*1*). The global population, now at 6.4 billion, is still growing rapidly and is projected to reach 8.9 billion people by 2050 (*2*). Cereals are an important source of calories for humans, both by direct intake and as the main feed for livestock. About 50% of the calories consumed by the world population originate from three cereals: rice (23%), wheat (17%), and maize (10%) (*3*). To meet the expanding food demands of the rapidly growing world population, crop grain production will need to increase by 50% by 2025 (*4*).

Many agronomically important traits, including yield, are expressed in continuous phenotypic variation. These complex traits usually are governed by a number of genes known as quantitative trait loci (QTLs) derived from natural variations (*5*). QTL analysis has been employed as a powerful approach to discover agronomically useful genes (*6–13*).

Rice (*Oryza sativa* L.) is a staple food and has been established as a model monocot because it has the smallest genome size (390 Mb) among the major cereals (*14*), because its genome is syntenic with the genomes of other cereals (*15*), and because rice can be transformed easily. As a result, many molecular markers for rice have been developed, many mutants have been generated and stocked, and the complete genome of rice has been mapped and sequenced (*14, 16–21*). These accomplishments have greatly facilitated QTL analysis in rice. Grain number and plant height are important traits that directly contribute to grain productivity. Dwarf rice and wheat varieties were developed by classical plant breeding methods, contributing to the green revolution in the 1960s. Higher yields were obtained from these dwarf crops because their short stature reduced lodging, which is an agronomic term for bending of plants toward the ground after wind or rain storms (*22–25*). During the past decade, many attempts have been made to characterize QTLs for grain production and plant height; however, the genes involved in these QTLs have not been identified yet, and their chromosomal positions remain obscure. We aimed to identify genes of QTLs for grain number and plant height, not only to elucidate molecular mechanisms that regulate grain productivity but also to use these genes for breeding.

QTL analysis. A choice of parental lines that show wide phenotypic variation in the targeted traits is necessary for QTL analysis, because QTL detection is based on natural allelic differences between parental lines. We chose an *indica* rice variety, Habataki, and a *japonica* variety, Koshihikari, because they not only exhibit large variations in agronomically important traits but also have many molecular markers available (*21*). On average, Habataki plants are shorter than individuals of Koshihikari but produce more grains in their main panicle (Fig. 1, A to D).

We developed primary-mapping populations of 96 backcross inbred lines (BILs) derived from the cross between Habataki and Koshihikari. Both grain number and plant height seemed to be regulated by QTLs, as these traits were approximately normally distributed in the mapping population (fig. S1). QTL analysis detected five QTLs for increasing *grain number* (*Gn*) and four QTLs for *plant height* (*Ph*) (Table 1 and Fig. 1E). The most effective QTL for plant height, *Ph1*, was located close to the *semi-dwarf 1* gene (*sd1*) that encodes gibberellin 20 oxidase (*23–25*). Comparison of *SD1* between Habataki and Koshihikari revealed that Habataki had a 383–base pair (bp) deletion in the coding region of *gibberellin 20 oxidase*. The resulting loss of function caused the reduced plant height in Habataki. The deletion in the *gibberellin 20 oxidase* is the same as the causal variation found in IR8, a variety that helped lead to the green revolution in rice (*23–25*).

The most effective QTL for increasing grain number, *Gn1* on chromosome 1, was selected for further analysis. The Habataki *Gn1* allele is expected to produce ~92 more grains per main panicle than the Koshihikari allele; *Gn1* explains 44% of the difference in grain number between Habataki and Koshihikari (Table 1). So far, several QTLs associated with yield have been reported in rice. Some of these QTLs are located near the *Gn1* region on the short arm of

[1]Bioscience and Biotechnology Center, Nagoya University, Nagoya 464-8601, Japan. [2]Plant Science Center, RIKEN, Tsurumi, Yokohama 230-0045, Japan. [3]Honda Research Institute Japan Co., Ltd., Kisarazu, Chiba, 292-0818 Japan. [4]China National Rice Research Institute, Hangzhou, 310006, China.

*These authors contributed equally to this work.
†To whom correspondence should be addressed.
E-mail: makoto@agr.nagoya-u.ac.jp

Supernova Olivine from Cometary Dust

Scott Messenger *et al.*

Science **309**, 737 (2005);
DOI: 10.1126/science.1109602

This copy is for your personal, non-commercial use only.